Euro. Jnl of Applied Mathematics (2007), *vol.* 17, *pp.* 607–631.
doi:10.1017/S0956792506006759 Printed in the United Kingdom

Free boundary Darcy flows with surface tension: Analytical and numerical study

Yu. A. SEMENOV[1] and L. J. CUMMINGS[2]

[1] *Institute of Hydromechanics of the NAS of Ukraine, Zhelyabov str. 8/4, 03057, Kiev, Ukraine*
email: semenov@a-teleport.com
[2] *School of Mathematical Sciences, University of Nottingham, Nottingham NG7 2RD, UK*

(*Received 24 May 2005; revised: 22 November 2006*)

We study surface tension effects for two-dimensional Darcy flow with a free boundary in a corner between two non-parallel walls. The analytic solution is based on two governing expressions constructed in an auxiliary parameter domain, namely a complex velocity and a derivative of the complex potential. These expressions admit a general solution for the problem in a corner geometry for the flow generated by a source/sink at the corner vertex or at infinity. We derive an integral equation in terms of the velocity modulus and angle at the free surface, determined by the dynamic boundary condition. A numerical procedure, used to solve the obtained system of equations, and numerical results concerning the effect of surface tension on the time evolution of the free boundary, are discussed.

1 Introduction

Two-dimensional flows with a free boundary governed by Darcy's law have been the subject of much research during the past few decades. This is due to the wide range of physical phenomena (e.g. crystal growth or dissolution [3], directional solidification or melting [38], electrochemical machining or forming [30], flow through a porous medium and filtration [2], Hele–Shaw flow [15]) whose interface dynamics (in appropriate physical limits) are governed by this mathematical model, subject to the same interface conditions.

A classical experimental setup for studying fluid motions under Darcy's law is the Hele–Shaw cell [17]: two parallel plates of glass or perspex, with a narrow gap between them. A syringe can be used to inject viscous fluid into, or suck fluid out of, the gap between the plates; or alternatively, air can be injected into a region already filled with viscous fluid. In the famous experiment of Saffman & Taylor [39] air is injected into one end of a rectangular Hele–Shaw cell already filled with viscous liquid, and the free boundary between the air and the viscous fluid is seen to form a travelling-wave "finger". The same experiment can be carried out in a radial geometry (either with [42, 29] or without [35, 42] confining wedge boundaries), and analogous radial fingering patterns, complicated by tip-splitting instabilities, are observed. The linear stability of the unconfined radial problem was first carried out by Bataille [1], and can explain the onset of the experimentally-observed fingering pattern; and the weakly nonlinear stability of Miranda & Widom [32]

predicts the onset of tip-splitting in these initial fingers. More general questions about the patterns observed in nonlinear fingering in the wedge geometry (with reference to the experiments of Thomé *et al.*) were addressed by Combescot & Ben Amar [8, 10].

It has long been known that the zero-surface-tension (ZST) Hele–Shaw problem in which a more viscous fluid is displaced by a less viscous one, such as air (the so-called "suction problem", since typically the more viscous fluid is being "sucked out"), is ill-posed (see [13]; also Howison *et al.* [24] and references therein). Arbitrarily small differences in initial interface shapes generally lead to radically different interface shapes even a short time later. Typically, though not always, solutions to the ZST suction problem undergo finite-time blow-up, developing singularities (usually cusps) in the free boundary [24]; examples of such blow-up solutions go back to 1945 [14, 36]. However, there are a large number of explicit analytical solutions, obtained by expressing the flow domain as the image under a conformal mapping of a fixed canonical domain, usually the unit disk, using ideas from complex analysis [14, 36] (conformal maps that are rational or log-rational functions can provide explicit solutions to the ZST free boundary problem). Most relevant for the present study is the family of explicit radial fingering solutions found by Howison [21] which, for appropriate choices of the parameters, can mimic beautifully the complex fingering patterns (including tip-splitting) observed by Paterson [35].

Another type of explicit (self-similar) solution to the ZST problem was proposed by Howison & King [23], who reduced the problem to the Poisson equation, eliminating time by applying the Baiocchi transformation [28], and then made use of a complex variable method due to Polubarinova-Kochina, originally developed to solve the dam seepage problem [37]. These solutions again express the free boundary in terms of a conformal mapping from a known auxiliary domain, but the conformal mapping is here given in terms of hypergeometric functions. Ben Amar [4, 5] also derived a family of explicit similarity solutions of this kind in a wedge geometry, though using different methods. Ben Amar's self-similar solutions, again for appropriate choices of the parameters, mimic the shapes (prior to tip-splitting) of the experimental fingers [42, 29].

Both these classes of fingering solutions [21, 4, 5] exist for all time. Their drawback from the physical point of view is that, within the ZST framework, there is no criterion for "selecting" which member of the solution family should be observed in a given experimental situation. The accepted "selection mechanism" for such cases is to introduce small positive (regularising) surface tension into the dynamic boundary condition, which reduces the continuum of solutions to a discrete set, one of which is the physically-relevant one. The procedure is known as regularisation because the modified suction problem, although still unstable, is no longer ill-posed. Solving for the regularised problem can be done numerically (as was done by McLean & Saffman [31] for the classical Saffman-Taylor finger), or using ideas from asymptotics "beyond all orders" (see elsewhere [19, 9, 41] for the Saffman–Taylor problem, and [8, 10, 6] for the radial fingering solutions of Ben Amar [4, 5]). Small surface tension acts as a singular perturbation to the ZST problem, and selection of solutions from a continuum of ZST solutions is governed by terms that are transcendentally small in the surface tension parameter.

For non-zero surface tension (the NZST problem), almost no analytical solutions exist, and the only way to generate solutions has been via sophisticated numerics. There have been several recent numerical studies investigating the regularising effect of surface tension

in the suction problem, and the tip splitting of fingers. The most commonly used approach is the boundary integral method used by Kelly & Hinch [25], Nie & Tian [33], Ceniceros *et al.* [7] and Dai & Shelley [12], who all investigated the interface dynamics of the unstable suction problem. Numerical results confirm the generally accepted hypothesis as to the behaviour of the fluid once surface tension forces are included: the solution exists well beyond the time of cusp formation for the corresponding zero surface tension problem, with the interface remaining smooth.

In this article we present a semi-analytical solution method for NZST Hele-Shaw flow in a corner (wedge), which allows us to solve the general problem for the flow generated by a source or sink at the corner vertex or at infinity. Our solution method follows that proposed by Zhukovskii [43] for steady jet flows of an ideal fluid, the key step being the analytical construction of two governing functions: the complex velocity, and the derivative of the complex potential defined in an auxiliary parameter domain. The problem is formulated in § 2, where these governing functions are derived. The expression for the complex velocity depends on the variation of the velocity modulus along the free boundary, and the derivative of the complex potential contains a function representing the angle that the velocity forms with the free surface. Both functions are given in terms of the auxiliary parameter variable u, which lies in a quarter-space corresponding to the physical flow domain. For a given initial free boundary shape we derive the integro-differential equation for the velocity modulus along the free boundary. This integral equation must be solved numerically to complete the solution. In § 3 the method of successive approximations adopted for solving the integral equation is outlined. Sample numerical results are given for the cases of a source and a sink at the corner vertex, and at infinity, for various values of the surface tension parameter.

The results for the ZST problem show the expected finite-time blow-up for the suction problem. However, for small positive surface tension, the calculation process is stable beyond the breakdown time of the corresponding ZST solution, and shows finger formation. With a sink at infinity, the finger grows faster as the surface tension is decreased, in line with linear stability analysis [1, 35], which predicts that the wavelength of the fastest-growing finger increases as surface tension is increased.

2 Statement of the problem

We consider the flow of viscous incompressible fluid in a wedge-shaped Hele-Shaw cell, generated by a homogeneous source/sink of constant strength Q in the vertex or at infinity, as shown in Figure 1. The flow region $\Omega(t)$ is a simply-connected domain bounded by the fixed walls CO and AC, and we denote the moving free boundary by $\Gamma(t)$, along which the pressure P varies according to the dynamic boundary condition. We assume that passive air, at ambient pressure $P_a(t)$, lies adjacent to $\Gamma(t)$ outside $\Omega(t)$. We take the origin of Cartesian coordinates (x, y) to lie at the corner vertex, such that the positive x-axis contains one of the wedge walls. The range of positive corner angles $0 < \alpha < 2\pi$ corresponds to the source/sink lying at the corner vertex (see Figure 1(a)), and the negative range $(-2\pi) < \alpha < 0$ corresponds to the source/sink lying at infinity (see Figure 1(b)).

https://doi.org/10.1017/S0956792506006759 Published online by Cambridge University Press

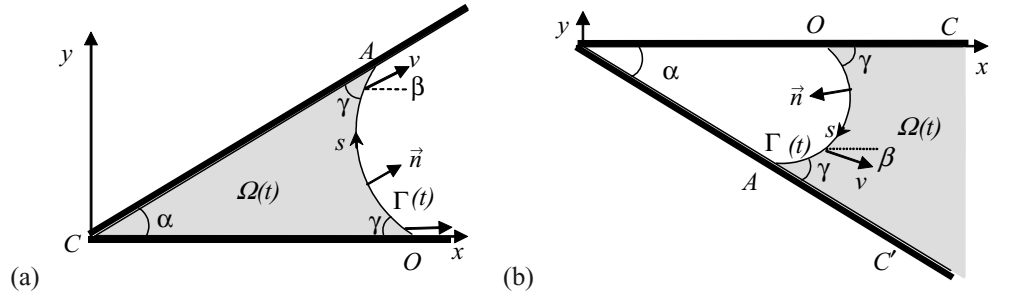

FIGURE 1. The flow region (a) in a bounded corner with the source/sink at the corner vertex; and (b) in an infinite corner with source/sink at infinity.

If the gap width in the Hele–Shaw cell is h, the flow averaged across the gap is governed by Darcy's law

$$\bar{\boldsymbol{U}} = -K\nabla P, \tag{2.1}$$

in the flow region $\Omega(t)$, where $\bar{\boldsymbol{U}} = (U_1, U_2)$ is the fluid velocity in the plane of the cell averaged across the gap (satisfying $\nabla \cdot \bar{\boldsymbol{U}} = 0$ for an incompressible fluid), and the permeability $K = h^2/(12\mu)$. (The relation (2.1) is also satisfied by flow in a porous medium with constant permeability K.) The surface tension affects the pressure jump across the interface according to the dynamic boundary condition

$$P - P_a(t) = \Sigma\chi \quad \text{on } \Gamma(t),$$

where Σ is the coefficient of surface tension and χ is the local curvature of $\Gamma(t)$ in the plane of the Hele-Shaw cell.

It is usual to work with the dimensionless variables $p = (K/(L^*U^*))(P - P_a)$ and $\bar{\boldsymbol{u}} = U^*\bar{\boldsymbol{U}}$, where L^* is a typical horizontal lengthscale of the flow, and U^* is a typical horizontal velocity scale, which will be given by $U^* = |Q^*|/(|\alpha|L^*)$ in our problem ($|Q^*|$ is a typical source/sink strength). Then, in dimensionless variables,

$$\bar{\boldsymbol{u}} = -\nabla p, \tag{2.2}$$

and p satisfies

$$\Delta p = 0 \quad \text{in} \quad \Omega(t)\backslash\{0\}, \quad \text{with} \tag{2.3}$$

$$p \sim -\frac{q}{\alpha}\log r \quad \text{as } r \to 0 \text{ for source/sink at origin, or} \tag{2.4}$$

$$p \sim -\frac{q}{\alpha}\log r \quad \text{as } r \to \infty \text{ for source/sink at infinity;} \tag{2.5}$$

$$\text{(a)} \quad p = \sigma\kappa, \quad \text{(b)} \quad \frac{\partial p}{\partial n} = -v_n \quad \text{on } \Gamma(t), \tag{2.6}$$

$$\frac{\partial p}{\partial n} = 0 \quad \text{on the wall sides } OC \text{ and } CA, \tag{2.7}$$

where $q = Q/|Q^*|$ is the dimensionless source/sink strength, r is radial distance from the wedge apex, $\sigma = \Sigma K/(L^{*2}U^*)$ is a dimensionless coefficient of surface tension, $\kappa = L^*\chi$ is the dimensionless curvature of the interface (positive if $\Omega(t)$ is convex), and v_n is the

https://doi.org/10.1017/S0956792506006759 Published online by Cambridge University Press

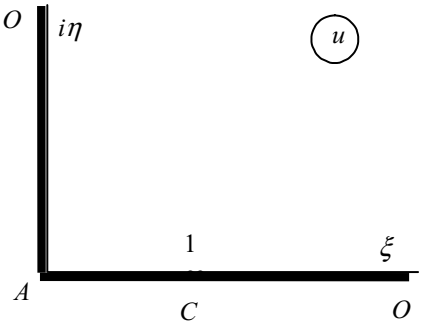

FIGURE 2. Parameter domain in the u-plane.

normal component of the (dimensionless) velocity of a liquid particle at the moving boundary.

The evolution of the free boundary $\Gamma(t)$ is determined by the kinematic condition (2.6). At the points A and O $\Gamma(t)$ meets the walls with contact angle γ (see figure 1), assumed to be constant and given by the physics of interaction of the fluid with the material of the walls. In the case of zero surface tension, $\sigma = 0$, γ must take the value $\pi/2$.[1]

Following [36, 14] (and many subsequent authors), we introduce a complex analytical potential $W(z,t) = -p(x,y,t)+i\psi(x,y,t)$, where $\psi(x,y,t)$ is the stream function conjugating $-p(x,y,t)$ harmonically. Then if $\bar{\boldsymbol{u}} = (v_1, v_2)$, equation (2.2) can be written as

$$v_1 + iv_2 = \overline{\frac{\partial W}{\partial z}},$$

thus $\partial W/\partial z$ is a complex conjugate velocity.

Instead of finding the mapping function $W = W(z,t)$ explicitly, we follow the method proposed by Zhukovskii [43], *i.e.* find two functions defined in an auxiliary parameter domain u: the complex conjugate velocity $\partial W/\partial z$, and the derivative of the complex potential, $\partial W/\partial u$. Then the function $z = z(u,t)$ mapping the domain in the u-plane onto the physical plane is obtained via

$$z(u,t) = z(0,t) + \int_0^u \frac{\partial W}{\partial u} \Big/ \frac{\partial W}{\partial z}\, du, \tag{2.8}$$

allowing us to find the solution in parametric form.

We choose the first quadrant of the u-plane to correspond to the physical domain $\Omega(t)$, where the complex variable $u = \xi + i\eta$. A conformal mapping allows us to fix the three points O, A and C as shown in figure 2, so that the interval $0 \leqslant \xi \leqslant 1$ of the real axis corresponds to the wall AC and the interval $1 \leqslant \xi \leqslant \infty$ corresponds to the wall CO. The imaginary η-axis of the parameter domain corresponds to the free boundary OA. Since the actual ranges of the complex velocity and complex potential are unknown *a priori*, an

[1] If $\sigma = 0$ then p is constant on $\Gamma(t)$, thus $\bar{\boldsymbol{u}}$ is perpendicular to $\Gamma(t)$, and the tangential velocity component is zero along $\Gamma(t)$, including at the wall intersection points A and O. On the other hand, at these points the velocity must be directed along the walls by the no-flux condition (2.7). It follows that when $\sigma = 0$, $\gamma = \pi/2$.

https://doi.org/10.1017/S0956792506006759 Published online by Cambridge University Press

explicit conformal transform of the first quadrant onto the complex velocity and complex potential planes is a difficult problem. At this stage, to find these functions, we assume that the velocity modulus and angle at the free boundary are known as functions of the parameter variable η.

2.1 Explicit expression for the complex velocity

We map implicitly the first quadrant of the u-plane onto the complex conjugate velocity plane using Chaplygin's singular point method [16]. It can be seen that the velocity at the point C tends to infinity (Figure 1(a)) or zero (Figure 1(b)), therefore at C the mapping is not conformal. With passage around C on an infinitesimal semicircle in the u-plane, the argument of $(u-1)$ changes by π (Figure 2), while the corresponding change in the argument of $\partial W/\partial z$ is $(-\alpha)$. The same property is possessed by $(u-1)^{-\alpha/\pi}$. With unidirectional flow driven from a single point singularity, there can be no other stagnation points, or points where the fluid velocity is infinite, in the flow domain. Thus, the complex velocity function $\partial W/\partial z$ has the singularity $(u-1)^{-\alpha/\pi}$ in the parameter domain, and no others.

We next assume that the velocity modulus on the free boundary is known; call it $v(\eta,t)$. Also, let the velocity modulus at the particular point O be $v_O(t)$. By the above observation about singularities, the function

$$F(u,t) := \frac{\operatorname{sgn}(\alpha q)}{v_O(t)}\left(\frac{u-1}{u+1}\right)^{\alpha/\pi}\frac{\partial W}{\partial z}(u)$$

is analytic on the first quadrant of the u-plane. On the boundary $u = i\eta$,

$$|F(u,t)|_{u=i\eta} = \frac{v(\eta,t)}{v_O(t)}.$$

The function $G(u,t) = -i\ln F(u,t)$ is then also a complex analytic function of u, whose real and imaginary parts $g_1(\xi,\eta)$ and $g_2(\xi,\eta)$ are harmonic functions, with $g_2(0,\eta) = -\ln|F| = -\ln(v/v_O)$, which we assume is known, and which decays at infinity by choice of the normalising factor $v_O(t)$. The function $G'(u,t) = g_{1\xi} + ig_{2\xi} \equiv g_{2\eta} - ig_{1\eta}$ is also a complex analytic function, whose harmonic real and imaginary parts satisfy the Cauchy-Riemann equations, with

$$g_{2\eta} = -\frac{\partial}{\partial\eta}(\ln v) \quad \text{on } \xi = 0.$$

By the assumption that the contact angle made by the free boundary with the wall at the point O is constant, we must have $\partial v/\partial\eta = 0$ at $\eta = 0$ (Appendix A). Thus we may extend the function $v(\eta,t)$ into $\eta < 0$ as an even function (so $\partial(\ln v)/\partial\eta$ is an odd function), and solve for functions on the entire half-plane $\xi \geqslant 0$.

In general, for a harmonic function $a_1(\xi,\eta)$ that decays as $\xi^2+\eta^2 \to \infty$, with boundary data $a_1(0,\eta) = \alpha_1(\eta)$, $\eta \in (-\infty,\infty)$ that is known to be odd in η, standard techniques [34, p.176] give the solution as

$$a_1(\xi,\eta) = \frac{\xi}{\pi}\int_0^\infty \frac{\alpha_1(\eta')d\eta'}{\xi^2+(\eta'-\eta)^2} - \frac{\xi}{\pi}\int_0^\infty \frac{\alpha_1(\eta')d\eta'}{\xi^2+(\eta'+\eta)^2}.$$

https://doi.org/10.1017/S0956792506006759 Published online by Cambridge University Press

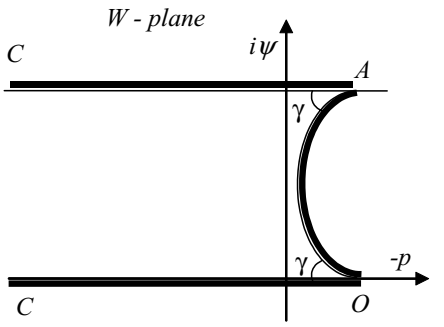

FIGURE 3. Plane of the complex potential. The image of the wall CA lies along $\psi = q$.

If a_2 denotes a harmonic conjugate function to a_1, such that a_1 and a_2 satisfy the Cauchy-Riemann equations, then a_2 is given by

$$a_2(\xi,\eta) = \frac{1}{\pi}\int_0^\infty \frac{(\eta'-\eta)\alpha_1(\eta')d\eta'}{\xi^2+(\eta'-\eta)^2} + \frac{1}{\pi}\int_0^\infty \frac{(\eta'+\eta)\alpha_1(\eta')d\eta'}{\xi^2+(\eta'+\eta)^2}.$$

Thus, for odd boundary data $\alpha_1(\eta)$, the complex analytic function $A(u)$ such that $A'(u) = a_1(\xi,\eta) + ia_2(\xi,\eta)$ may be seen to satisfy

$$A(u) = \frac{1}{\pi}\int_0^\infty \alpha_1(\eta')\ln\left(\frac{u-i\eta'}{u+i\eta'}\right)d\eta',$$

up to an additive constant.

We apply this result to obtain the solution for the function $G(u,t)$ defined above, using the fact that $g_{2\eta}(0,\eta)$, the boundary data for the real part of $G'(u)$, must be an odd function of η. It follows that

$$G(u,t) = -\frac{1}{\pi}\int_0^\infty \frac{\partial(\ln v)}{\partial\eta'}\ln\left(\frac{u-i\eta'}{u+i\eta'}\right)d\eta',$$

and hence, using the definition of $G = -i\ln F$, that

$$\frac{\partial W}{\partial z} = \mathrm{sgn}(\alpha q)v_O(t)\left(\frac{u+1}{u-1}\right)^{\alpha/\pi}\exp\left(\frac{-i}{\pi}\int_0^\infty \frac{\partial(\ln v)}{\partial\eta'}\ln\left(\frac{u-i\eta'}{u+i\eta'}\right)d\eta'\right) \tag{2.9}$$

(the term $\mathrm{sgn}(\alpha q)$ generalizes both cases (a) and (b) shown in figure 1).

2.2 Explicit expression for the complex potential

The imaginary part of the complex potential ψ changes from zero along the wall CO up to the value $\psi = q$ along CA. Therefore, the flow region in the W-plane takes the form shown in figure 3, while the regions in the z- and u-planes are as in Figures 1 and 2. The complex potential $W(u)$ thus has singularities at the points $u = 0, 1, \infty$, where it has the

https://doi.org/10.1017/S0956792506006759 Published online by Cambridge University Press

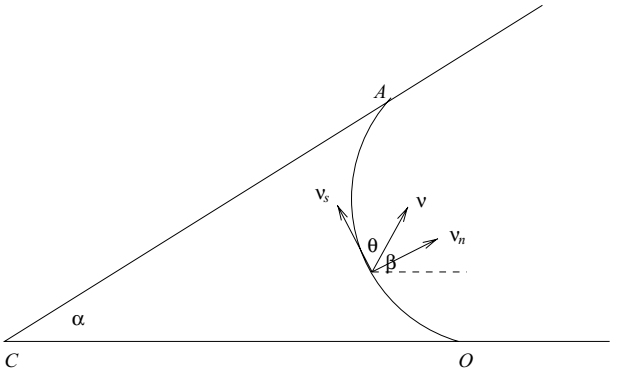

FIGURE 4. Definition sketch of the angles θ and β in the case of a source at the wedge vertex ($q > 0$, $\alpha > 0$), and the velocity vector at the free surface. The other cases for q and α may be sketched similarly.

local behaviour

$$\begin{aligned} W'(u) &\sim -\lambda_A u^{2\gamma/\pi-1} \quad \text{as } u \to 0 \ (A), \\ W'(u) &\sim \lambda_O u^{-2\gamma/\pi-1} \quad \text{as } u \to \infty \ (O), \\ W'(u) &\sim \frac{q}{\pi(u-1)} \quad \text{as } u \to 1 \ (C), \end{aligned} \tag{2.10}$$

for real positive functions of time λ_A, λ_O. This behaviour is readily deduced by considering the local form that the conformal mapping between Figures 2 and 3 must take at each of these singular points. There are no other points in the u-plane where the mapping is not conformal.

To analyse the behaviour of W along the free surface it is useful to introduce the unit vectors $\boldsymbol{n} = (n_1, n_2)$ and $\boldsymbol{\tau} = (\tau_1, \tau_2)$, normal (in the direction away from the fluid) and tangential (in the direction of increasing arclength s in Figure 1) respectively to the free surface. Let θ denote the angle between the velocity vector $\boldsymbol{v}$ on the free surface and the unit vector $\boldsymbol{\tau}$, such that the normal and tangential components of velocity at the free surface, v_n and v_s, are given by

$$v_n = v \sin\theta, \quad v_s = v \cos\theta. \tag{2.11}$$

For the case $q > 0$, the angle θ varies between the values γ and $(\pi - \gamma)$, with $\theta_A = \gamma$ and $\theta_O = \pi - \gamma$, as is sketched in Figure 4 for the case $\alpha > 0$. For $q < 0$ the situation is slightly different; θ varies between $(\gamma - \pi)$ and $-\gamma$, with $\theta_A = \gamma - \pi$ and $\theta_O = -\gamma$. (θ is negative in this case as the velocity component v_n is in the opposite direction to the defined outward normal vector, and hence is negative, while the velocity modulus v is always positive.) We also introduce the angle β made by the velocity vector at the free surface with the wall CO, again indicated in Figure 4 for the case $\alpha > 0$, $q > 0$.

In complex form, $\tau_1 + i\tau_2 = \partial z/\partial s$ and $n_1 + i n_2 = -i\partial z/\partial s$, where $\partial z/\partial s = \exp(i(\beta + \theta))$ (s is arclength along the free boundary as denoted in Figure 1), and in terms of the conformal mapping,

$$\frac{\partial z}{\partial s} = i z'(i\eta)\frac{d\eta}{ds} = -\frac{i z'(i\eta)}{|z'(i\eta)|} \tag{2.12}$$

https://doi.org/10.1017/S0956792506006759 Published online by Cambridge University Press

(we know that $|\partial z/\partial s| = 1$, and that $d\eta/ds$ is real and negative). The complex conjugate velocity at the free boundary is given by

$$\left.\frac{dW}{dz}\right|_{bdy} = ve^{-i\beta}. \tag{2.13}$$

It follows, using (2.12) and the remarks preceding it, that

$$W'(i\eta) = \left.W'(z)\right|_{bdy} z'(i\eta) = ive^{i\theta}|z'(i\eta)|. \tag{2.14}$$

For the moment we assume that θ is a known function of the parameter variable η. Consider the complex function

$$H(u) = \log\left[M\frac{\partial W}{\partial u}(u^2-1)u^{1-2\gamma/\pi}\right],$$

for some real positive M. From (2.10) it follows that H is complex analytic on the first u-quadrant, and if $H(u) = H_1(\xi,\eta) + iH_2(\xi,\eta)$ and $H'(u) = h_1(\xi,\eta) + ih_2(\xi,\eta)$, then $h_1 = H_{1\xi} = H_{2\eta}$, and $h_2 = H_{2\xi} = -H_{1\eta}$. To fix ideas, suppose we have the case of a point source at the origin (other cases follow similarly). On $1 < \xi < \infty$, the wall CO, the flow velocity is parallel to the wall along the positive x-axis, thus the complex conjugate velocity $\partial W/\partial z \in \mathbb{R}^+$. Consideration of the local conformal map gives $\partial z/\partial u = \partial z/\partial\xi \in \mathbb{R}^+$, and so we have

$$\frac{\partial W}{\partial u} = \frac{\partial W}{\partial z}\frac{\partial z}{\partial u} \in \mathbb{R}^+, \quad 1 < \xi < \infty.$$

On $0 < \xi < 1$, the wall AC, the complex conjugate velocity is of the form $\partial W/\partial z = (+\text{ve})e^{-i\alpha}$, while the local conformal map is of the form $z \sim (+\text{ve})(u-1)^{\alpha/\pi}$. Thus

$$\frac{\partial W}{\partial u} = \frac{\partial W}{\partial z}\frac{\partial z}{\partial u} \in \mathbb{R}^-.$$

It follows that H_2, the imaginary part of H, is constant on each portion of the ξ-axis, and hence that $h_2(\xi,0) = 0$ for $\xi \in \mathbb{R}^+$, $\xi \neq 1$, and hence that $h_{1\eta}(\xi,0) = 0$. We can thus extend $h_{1\eta}(\xi,\eta)$ into $\eta < 0$ as an odd function of η, and $h_1(\xi,\eta)$ as an even function of η, and solve on the half-plane $\xi > 0$ if we also extend the boundary data $h_1(0,\eta)$. Using the result (2.14) we find that

$$H(i\eta) = \log\left[(+\text{ve})e^{i(\theta-\gamma)}\right]$$

(the angle θ as defined in (2.11)), and hence $H_2(0,\eta) = \theta - \gamma$, and

$$h_1(0,\eta) = \frac{\partial\theta}{\partial\eta}.$$

In general, for a complex analytic function $A(u) = A_1(\xi,\eta) + iA_2(\xi,\eta)$, if $A_{2\eta}$ is an even function then standard techniques [34, p.177] give the solution for A on the half-space

https://doi.org/10.1017/S0956792506006759 Published online by Cambridge University Press

$\xi > 0$ as

$$A(u) = \frac{1}{\pi}\int_0^\infty \frac{\partial A_2}{\partial \eta}(0,\eta')\ln(u^2+\eta'^2)\,d\eta'.$$

Applying this result (assuming θ is a known function of η), we obtain the solution for the complex analytic function $H(u)$ as

$$H(u) = \frac{1}{\pi}\int_0^\infty \frac{\partial \theta}{\partial \eta'}\ln(u^2+\eta'^2)\,d\eta',$$

giving the derivative of the complex potential as

$$\frac{\partial W}{\partial u} = \frac{Nu^{2\gamma/\pi-1}}{(u^2-1)}\exp\left(\frac{1}{\pi}\int_0^\infty \frac{\partial \theta}{\partial \eta'}\ln(u^2+\eta'^2)\,d\eta'\right). \tag{2.15}$$

The scale factor $N = 1/M$ is as yet arbitrary here; we fix it by imposing the residue theorem condition

$$2iq = \oint \frac{\partial W}{\partial u}du = iN\pi\exp\left(\frac{1}{\pi}\int_0^\infty \frac{\partial \theta}{\partial \eta'}\ln(\eta'^2+1)\,d\eta'\right),$$

where the complex integral is taken along any contour surrounding the point $u = 1$ (but excluding points $u = 0, -1$) in the parameter plane. The conformal map $W(u)$ from the parameter domain onto the corresponding domain in the complex potential plane can be obtained, if required, by integration of (2.15).

By substituting from (2.9) and (2.15) in (2.8) we can find the function $z(u,t)$ mapping the first quadrant onto the flow domain $\Omega(t)$ in the physical plane,

$$z(u,t) = z_A(t) + \int_0^u \frac{\partial z}{\partial u}du, \tag{2.16}$$

where $z_A(t)$ is the location of the point A, and

$$\begin{aligned}\frac{\partial z}{\partial u} &= \frac{\partial W}{\partial u}\Big/\frac{\partial W}{\partial z}\\ &= \frac{|N|\mathrm{sgn}(\alpha)}{v_O(t)(u^2-1)}\left(\frac{u-1}{u+1}\right)^{\alpha/\pi}\exp\left(\frac{i}{\pi}\int_0^\infty \frac{\partial(\ln v)}{\partial \eta'}\ln\left(\frac{u-i\eta'}{u+i\eta'}\right)d\eta'\right)\\ &\qquad \exp\left(\frac{1}{\pi}\int_0^\infty \frac{\partial \theta}{\partial \eta'}\ln(\eta'^2+u^2)d\eta'\right).\end{aligned} \tag{2.17}$$

The function $z = z(u,t)$ obtained from (2.16), (2.17) depends on the unknown functions of the velocity modulus $v(\eta,t)$ and velocity angle $\theta(\eta,t)$ on the free boundary, which must be determined from the given initial shape of the free boundary and dynamic and kinematic boundary conditions.

2.3 Basic integral equation

To determine the instantaneous free boundary shape, we set $u = i\eta$. The complex conjugate velocity is given by (2.13) at the free boundary, where $\beta = \beta(\eta,t)$ is defined in Figure 4.

https://doi.org/10.1017/S0956792506006759 Published online by Cambridge University Press

From equations (2.9) and (2.13) it follows that

$$\beta(\eta,t)=\frac{\pi}{2}\big(1-\operatorname{sgn}(\alpha q)\big)+\alpha-\frac{2\alpha}{\pi}\tan^{-1}\eta+\frac{1}{\pi}\int_0^\infty\frac{\partial(\ln v)}{\partial\eta'}\ln\left|\frac{\eta-\eta'}{\eta+\eta'}\right|d\eta'. \tag{2.18}$$

By setting $u=i\eta$ in (2.15) and using the boundary condition $\theta(0,t)=\gamma$ (for $q>0$) to evaluate the integral containing the imaginary part of the logarithm, we obtain

$$\frac{\partial W}{\partial\eta}=-N\frac{\eta^{\frac{2\gamma}{\pi}-1}}{(1+\eta^2)}\exp\left(\frac{1}{\pi}\int_0^\infty\frac{\partial\theta}{\partial\eta'}\ln\left|\eta'^2-\eta^2\right|d\eta'+i\theta(\eta,t)\right). \tag{2.19}$$

For the point sink case $q<0$ the condition $\theta(0,t)=\gamma-\pi$ leads to the factor $i\theta(\eta,t)$ in (2.19) being replaced by $i\theta(\eta,t)+i\pi$, and hence the whole expression changes sign in this case. Thus the two cases can be combined by replacing $(-N)$ on the right-hand side by $(-|N|)$. The interface shape is determined by equation (2.16) on the free boundary,

$$z(i\eta,t)=z_A(t)+\int_0^\eta\frac{\partial z}{\partial\eta'}d\eta', \tag{2.20}$$

where (combining both $q>0$ and $q<0$ results and noting that $\operatorname{sgn}(N)\equiv\operatorname{sgn}(q)$)

$$\frac{\partial z}{\partial\eta}=\frac{\partial W}{\partial\eta}\Big/\frac{\partial W}{\partial z}=-\frac{|N|\eta^{\frac{2\gamma}{\pi}-1}}{v(1+\eta^2)}\exp\left(\frac{1}{\pi}\int_0^\infty\frac{\partial\theta}{\partial\eta'}\ln\left|\eta'^2-\eta^2\right|d\eta'\right)e^{i(\beta+\theta)}. \tag{2.21}$$

Writing $\delta=\beta+\theta$ for the free boundary slope, we have $\partial z/\partial s=e^{i\delta}$, and we can recast the last expression as

$$\frac{\partial z}{\partial\eta}=\frac{\partial s}{\partial\eta}e^{i\delta}, \tag{2.22}$$

where

$$\frac{\partial s}{\partial\eta}=-\frac{|N|\eta^{\frac{2\gamma}{\pi}-1}}{v(1+\eta^2)}\exp\left(\frac{1}{\pi}\int_0^\infty\frac{\partial\theta}{\partial\eta'}\ln\left|\eta'^2-\eta^2\right|d\eta'\right). \tag{2.23}$$

If the velocity modulus v is known, then equation (2.20) determines the free boundary. Suppose the shape of the free boundary is given by the slope $\delta(s,t)$, then the velocity modulus $v(\eta,t)$, is determined as follows. Since $s=s(\eta,t)$, differentiating the expression $\delta=\beta+\theta$ with respect to η we have

$$\frac{\partial\beta}{\partial\eta}+\frac{\partial\theta}{\partial\eta}=\kappa\frac{\partial s}{\partial\eta}, \tag{2.24}$$

where $\kappa=\partial\delta/\partial s$ is the curvature of the free boundary. Substituting for $\partial\beta/\partial\eta$ (from (2.18)) and $\partial s/\partial\eta$ (from (2.23)) in (2.24), we obtain the following integral equation, including two unknown functions, $\partial(\ln v)/\partial\eta$ and $\partial\theta/\partial\eta$:

$$\begin{aligned}\frac{2}{\pi}\int_0^\infty\frac{\partial(\ln v)}{\partial\eta'}\frac{\eta'}{\eta'^2-\eta^2}d\eta'=&-\frac{2\alpha}{1+\eta^2}+\frac{\partial\theta}{\partial\eta}+\\&\frac{\kappa|N|\eta^{\frac{2\gamma}{\pi}-1}}{v(1+\eta^2)}\exp\left(\frac{1}{\pi}\int_0^\infty\frac{\partial\theta}{\partial\eta'}\ln\left|\eta'^2-\eta^2\right|d\eta'\right),\end{aligned} \tag{2.25}$$

https://doi.org/10.1017/S0956792506006759 Published online by Cambridge University Press

where

$$v(\eta,t)=v_O(t)\exp\left(-\int_\eta^\infty\frac{\partial(\ln v)}{\partial\eta'}d\eta'\right).$$

2.4 Dynamic boundary condition

The surface tension leads to the pressure jump across the interface $\Gamma(t)$ according to condition (2.6(a)), which in terms of the complex potential is

$$\Re\left[W(i\eta)\right]=-\sigma\kappa.$$

Assuming isotropic surface tension, differentiating with respect to η and using (2.19) (generalised to both source and sink cases) gives

$$\frac{|N|\eta^{\frac{2\gamma}{\pi}-1}\cos\theta}{1+\eta^2}\exp\left(\frac{1}{\pi}\int_0^\infty\frac{\partial\theta}{\partial\eta'}\ln|\eta'^2-\eta^2|d\eta'\right)=\sigma\frac{\partial\kappa}{\partial\eta}=\sigma\frac{\partial\kappa}{\partial s}\frac{\partial s}{\partial\eta},$$

or

$$\text{(a)}\quad v\cos\theta=-\sigma\frac{\partial\kappa}{\partial s},\quad\text{(b)}\quad v\sin\theta=\mathrm{sgn}(q)\sqrt{v^2-\sigma^2\left(\frac{\partial\kappa}{\partial s}\right)^2},\tag{2.26}$$

where (2.23) was used to obtain (2.26(a)). Recalling (2.11), this is equivalent to $v_s=-\sigma(\partial\kappa/\partial s)$, i.e. the tangential component of the velocity is determined by the derivative of the curvature along the free boundary. At the contact points, $\theta_A=\gamma$ and $\theta_O=\pi-\gamma$ ($q>0$), and $\theta_A=\gamma-\pi$, $\theta_O=-\gamma$ ($q<0$). Equation (2.26(a)) thus gives the relations

$$\frac{\partial\kappa}{\partial s}=\mp\mathrm{sgn}(q)\frac{v\cos\gamma}{\sigma}\quad\text{at}\begin{cases}A\\O.\end{cases}\tag{2.27}$$

Note that, if the contact angle $\gamma=\pi/2$, then $\partial\kappa/\partial s=0$ at the intersection points.

Differentiating the function

$$\theta=\arccos\left(-\frac{\sigma}{v}\frac{\partial\kappa}{\partial s}\right)$$

with respect to η using (2.26(b)) gives

$$\frac{\partial\theta}{\partial\eta}=\frac{\sigma\mathrm{sgn}(q)}{v\sin\theta}\left(\frac{\partial^2\kappa}{\partial s^2}\frac{\partial s}{\partial\eta}-\frac{\partial(\ln v)}{\partial\eta}\frac{\partial\kappa}{\partial s}\right),\tag{2.28}$$

and substituting (2.28) into (2.21) we can reduce the boundary value problem (2.3)–(2.7) to an integral equation for the velocity modulus $v(\eta,t)$, if the curvature $\kappa=\kappa(s,t)$ (determined by the flow kinematics) is known at each instant of time.

https://doi.org/10.1017/S0956792506006759 Published online by Cambridge University Press

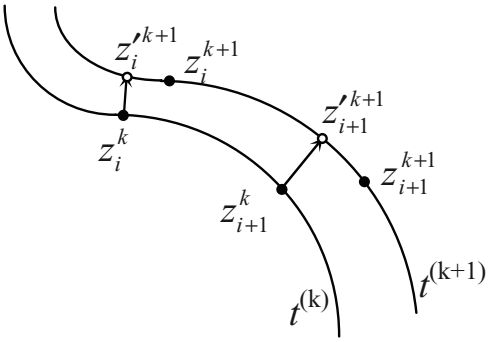

FIGURE 5. Explicit scheme of time integration.

2.5 Kinematic boundary condition

The velocity of a point of the free boundary must be equal to the velocity of the fluid at that point of the free boundary. This condition can be expressed as follows:

$$\frac{dz}{dt} = \frac{\partial z}{\partial t} + \frac{\partial z}{\partial \eta}\frac{d\eta}{dt} = v e^{i\beta} \quad \text{on } \Gamma(t), \tag{2.29}$$

or, considering the free boundary position as $z = z(s(\eta, t), t)$ and using $\partial z/\partial s = e^{i\delta} \equiv e^{i(\beta+\theta)}$,

$$\frac{\partial z}{\partial t} = v e^{i\beta} - \frac{\partial s}{\partial \eta}\frac{d\eta}{dt} e^{i(\beta+\theta)} \quad \text{on } \Gamma(t), \tag{2.30}$$

from which we obtain the 'Polubarinova-Galin' type equation [36, 14]

$$\Im\left[e^{-i\theta}\left(\frac{\partial z}{\partial t}\Big/\overline{\frac{\partial W}{\partial z}} - 1\right)\right] = 0 \quad \text{on } \Gamma(t). \tag{2.31}$$

This equation (2.31) taken together with (2.9) and (2.20) leads to a rather complicated integral equation. Instead of solving this equation numerically, we use the kinematic boundary condition in Lagrangian form (2.29), as sketched in Figure 5. Let the η_i, $i = 1, \ldots, n$ be a fixed set of points distributed along the imaginary axis of the parameter domain. Equation (2.20) determines the corresponding points $z_i^{(k)} = z^{(k)}(\eta_i, t)$ of the free boundary at time $t^{(k)}$. The liquid particles associated with points $z_i^{(k)}$ move with the known velocity $v_i^{(k)} e^{i\beta_i^{(k)}}$, and at time $t^{(k+1)} = t^{(k)} + \Delta t$ (where Δt is the time step) take position

$$z_i'^{(k+1)} = z_i^{(k)} + v_i^{(k)} e^{i\beta_i^{(k)}} \Delta t. \tag{2.32}$$

The free boundary shape at time $t^{(k+1)}$ is given by the set of points $z_i'^{(k+1)}$. Applying an approximation procedure (splining, in our case) to these points, and differentiating the obtained function $z^{(k+1)} = z(s^{(k+1)}, t)$ with respect to s, we can determine the curvature and its first and second derivatives at time $t = t^{(k+1)}$, which appear in the right-hand side of integral equations (2.25) and (2.28). Solving these equations for the functions $\partial(\ln v)/\partial\eta$ and $\partial\theta/\partial\eta$, we can determine the velocity modulus $v(\eta, t)$, and the velocity direction $\beta(\eta, t)$ from equation (2.18), for time $t = t^{(k+1)}$. The new position of the points

https://doi.org/10.1017/S0956792506006759 Published online by Cambridge University Press

$z_i^{(k+1)} = z^{(k+1)}(\eta_i, t)$ can be determined either by integrating equation (2.20), or by using the obtained approximation $z_i^{(k+1)} = z(s_i^{(k+1)}, t)$, where the coordinates s_i are determined as follows

$$s_i^{(k+1)} = \int_0^{\eta_i} \left| \frac{\partial z}{\partial \eta} \right|^{(k+1)} d\eta.$$

The unknown velocity $v_O(t^{(k+1)})$ in equation (2.25) (it appears via the expression for $v(\eta, t)$) is determined from the condition

$$S^{(k+1)} = s_n^{(k+1)}, \tag{2.33}$$

where $S^{(k+1)}$ is the total length of the free boundary for time $t = t^{(k+1)}$.

It should be noted that the applied explicit time integration method requires a smaller time step, $\Delta t < C\Delta s_i^2$, than implicit methods of higher orders [20]. On the other hand, the explicit time integration method allows us to solve only the integral equation (2.25) at each time step, for which we have developed an effective numerical procedure (presented in the following section). In addition, the number of iterations for solving (2.25) decreases linearly with decreasing the time step, since the right-hand side of the equations changes more slowly. Thus, the total time of calculations depends only weakly on the choice of time step.

3 Numerical method and results

In discrete form the solution is enforced on a fixed set of points η_i, $i = 1, \ldots, n$ distributed along the imaginary axis of the parameter domain with $\eta_1 = 10^{-6}$ and $\eta_n = 10^6$ so as to provide a uniform distribution of points z_i along the boundary in the physical plane (this is important for a precise approximation of the free boundary). During time evolution of the free boundary the points z_i move along the boundary, which may lead to a differential clustering of points along the boundary. At such times a new set of points η_i are re-generated, to provide again a uniform distribution points z_i. The total number of points was chosen in the range $n = 220$ — 440 to check the convergence of the solution of equation (2.25). For all calculated examples here the difference between the results for the indicated ranges of n and time step is smaller than could be distinguished in the figures. The curvature κ, and its derivatives $\partial\kappa/\partial s$ and $\partial^2\kappa/\partial s^2$, were calculated numerically by applying a spline approximation of tenth order to the discrete points z_i' forming the free boundary at time $t = t^{(k+1)}$. The boundary conditions at the intersection points O and A, i.e. the given value of the contact angle γ and the condition (2.27), were enforced, and we were able to obtain a precise enough approximation with the number of spline nodes $m = n/10$. This relation represents a compromise between the precision of approximation of the free boundary, and its smoothing which is necessary to compute the curvature and its derivatives numerically.

The solution of equations (2.25) and (2.28) was found using the method of successive approximations, applying the Hilbert transform to determine the $(k+1)$th approximation

$$\left(\frac{\partial(\ln v)}{\partial \eta} \right)^{(k+1)} = \frac{4}{\pi^2} \int_0^{\infty} K^{(k)}(\eta', t) \frac{\eta' d\eta'}{(\eta'^2 - \eta^2)(1 + \eta'^2)}, \tag{3.1}$$

https://doi.org/10.1017/S0956792506006759 Published online by Cambridge University Press

where

$$K^{(k)}(\eta,t) = -2\alpha + (1+\eta^2)\left(\frac{\partial\theta}{\partial\eta}\right)^{(k)} + \frac{\kappa|N|}{v^{(k)}}\eta^{\frac{2\gamma}{\pi}-1}\exp\left(\frac{1}{\pi}\int_0^\infty \left(\frac{\partial\theta}{\partial\eta'}\right)^{(k)} \ln\left|\eta'^2-\eta^2\right| d\eta'\right),$$

$$\left(\frac{\partial\theta}{\partial\eta}\right)^{(k)} = -\frac{\sigma\,\mathrm{sgn}(q)}{v^{(k)}\sin\theta}\left(\left(\frac{\partial(\ln v)}{\partial\eta}\right)^{(k)}\frac{\partial\kappa}{\partial s} - \frac{\partial^2\kappa}{\partial s^2}\left(\frac{\partial s}{\partial\eta}\right)^{(k)}\right),$$

$$\left(\frac{\partial s}{\partial\eta}\right)^{(k)} = -\left|N^{(k)}\right|\frac{\eta^{\frac{2\gamma}{\pi}-1}}{v^{(k)}(1+\eta^2)}\exp\left(\frac{1}{\pi}\int_0^\infty \left(\frac{\partial\theta}{\partial\eta'}\right)^{(k)} \ln\left|\eta'^2-\eta^2\right| d\eta'\right),$$

$$v^{(k)}(\eta,t) = v_O(t)\exp\left(-\int_\eta^\infty \left(\frac{\partial(\ln v)}{\partial\eta'}\right)^{(k)} d\eta'\right).$$

The selected numerical calculations presented here were carried out for initial shapes of the form

$$z(s,0) = z_A(0) + \int_0^s e^{i\delta(s')}ds', \tag{3.2}$$

with the free boundary slope given by

$$\delta(s) = \alpha\left(1 - s/s_{\max}\right) + C\sin\left(2\pi k s/s_{\max}\right), \tag{3.3}$$

where the value of the coefficient C and the wave number k are given in the figure captions. The chosen initial shapes satisfy (2.27) and are symmetric about the wedge centreline. They should remain so at future times, which provides us with some check on the accuracy of the results.

The solution presented generalizes both source and sink cases at the corner vertex or at infinity; however, we present only calculations for the more interesting suction cases (for the injection case the free boundary tends to a circle [40]).

Figure 6 shows the initial shape of the free boundary given by equations (3.2), (3.3) with $C = 0.4$ and $k = 2$, and the corresponding initial velocity distribution with and without surface tension for the case of a sink at infinity. It can be seen that the surface tension force increases the velocity modulus near the intersection points and at the fjord (the wedge centreline where the curvature is maximum), and decreases the velocity at the tips of fingers. At the inflection points (where the derivative of the curvature is maximum) the surface tension leads to maximum deviation of the velocity direction.

We may compare our numerical results with the experimental results of Lajeunesse & Couder [29]. These authors studied viscous fingering in the Hele–Shaw cell with corner geometry, and the same tip-splitting phenomenon was observed as in the earlier radial experiments of Paterson [35] and Thomé [42]. Figure 7 shows (a) the calculated and (b) the experimental evolution of the free boundary, for the corner angle $\alpha = -5\pi/9$. Although the initial shapes differ at the points of intersection with the wedge boundary,

https://doi.org/10.1017/S0956792506006759 Published online by Cambridge University Press

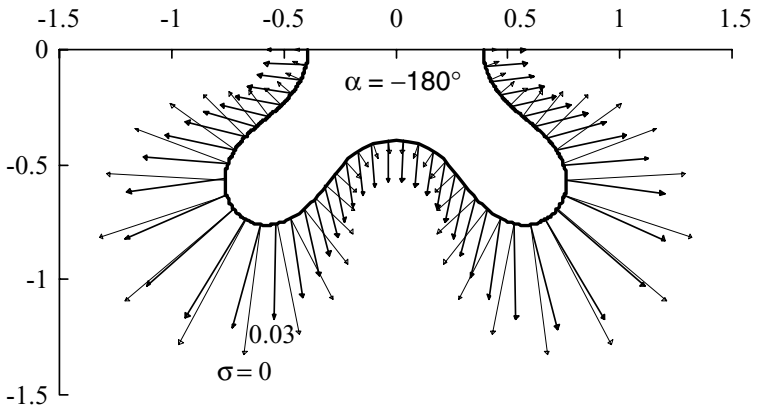

FIGURE 6. Effect of surface tension on the initial velocity distribution with a sink at infinity. The initial boundary is given by equations (3.2) and (3.3), with $C = 0.4$ and $\alpha = -\pi$. The thin and thick arrows correspond to $\sigma = 0$ and 0.03 respectively.

both show two small fingers, which develop during the evolution. Figure 7(c) shows the curvature at the (initial) fingertips ($s/s_{\max} = 0.25, 0.75$). This curvature, which is initially negative, decreases for $0 < t < 0.4$ and then increases for all later times. At some time it becomes zero, heralding the tip-splitting with the appearance of two new fjords, exactly at the tips of the old fingers. Despite the difference in initial conditions, the numerical simulation is qualitatively very similar to the experimental results reproduced in Figure 7(b).

It is worth noting that the plot of the derivative of the curvature versus dimensionless arc length along the free boundary, shown in Figure 7(d), has invariant "nodes" where $\partial\kappa/\partial s$ is zero, corresponding to maxima or minima of the curvature, *i.e.* finger tips or fjords in the physical plane. The behaviour of the curvature and its derivative at earlier times near these nodes can forecast the tip-splitting. For two 'waves' ($k = 2$ in (3.3)) we have four symmetric intervals of the free boundary, which persist in time in Figure 7(a), (c), (d). From Figure 7(c) and (d) we can see the difference between the interface dynamics at the finger-tips and at the fjords. The finger-tips are negative curvature minima (the fluid interface is locally concave), while the fjords are positive curvature maxima (fluid interface locally convex). At the fjords ($s/s_{max} = 0, 0.5, 1$) the second derivative of the curvature (the slope of $\partial\kappa/\partial s$ in Figure 7(d)) is positive initially and increases further over all calculated time, thus these initial fjords persist. At the finger-tips ($s/s_{max} = 0.25, 0.75$) the second derivative of the curvature is negative initially but also increases over time, and so becomes positive. Thus at the finger-tips $|\partial^2\kappa/\partial s^2|$ decreases in the time interval $0 < t < 0.4$, becomes zero at $t \approx 0.4$, and then starts to increase. Such behaviour leads to the appearance of new curvature maxima (fjords), or more precisely, the curvature minima at $s/s_{max} = 0.25, 0.75$ become curvature maxima, passing first through inflection points. Necessarily, two new curvature minima (fingertips) are created on either side of these new curvature maxima. These new minima of the curvature increase, as do the curvature maxima at $s/s_{max} = 0.25, 0.75$, causing the finger-tips to flatten. This continues until these maxima pass through zero and become positive, at which instant the interface becomes locally convex at these two points; the finger-tips split and become new fjords,

https://doi.org/10.1017/S0956792506006759 Published online by Cambridge University Press

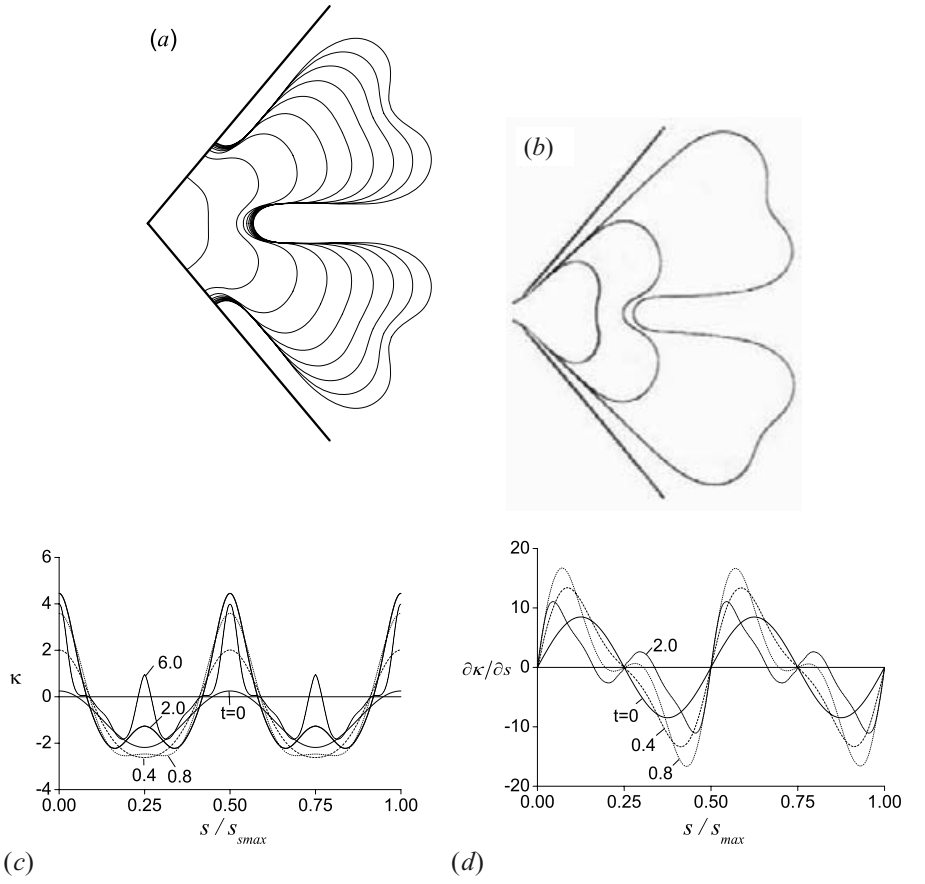

FIGURE 7. Effect of surface tension in the corner $\alpha = -5\pi/9$ (a) the evolving free boundary for $\sigma = 0.005$ (time interval 1.0 between successive contours); (b) experimental results of Lajeunesse and Couder [29];(c) evolution of the curvature ; and (d) derivative of the curvature, illustrating the fixed "nodes" at which $\partial\kappa/\partial s = 0$. The initial free boundary is given by (3.2), (3.3) with $C = 0.1\alpha$ and $k = 2$.

surrounded on either side by two new finger-tips corresponding to the curvature minima in the intervals $s/s_{max} \in (0, 0.25)$, $(0.25, 0.5)$, $(0.5, 0.75)$, $(0.75, 1)$, and the process is repeated.

Figures 8 and 9 show the effect of different values of surface tension: a larger value of σ slows the finger development, as predicted by the linear stability analysis of an expanding bubble in a radial Hele–Shaw cell [1, 35]. Such analysis for the problem laid out in (2.3)–(2.7) (for the sink at infinity) reveals that small perturbations to an expanding circular bubble with boundary $r = R_0(t)$, pressure $p = p_0(r, t)$, where

$$\left.\begin{aligned} p_0(r,t) &= -\tfrac{q}{\alpha}\log\left(\frac{r}{R_0(t)}\right) - \frac{\sigma}{R_0(t)} \\ R_0(t) &= \left(\tfrac{2qt}{\alpha} + R_0(0)\right)^{1/2} \end{aligned}\right\} \quad (q < 0,\ \alpha < 0),$$

https://doi.org/10.1017/S0956792506006759 Published online by Cambridge University Press

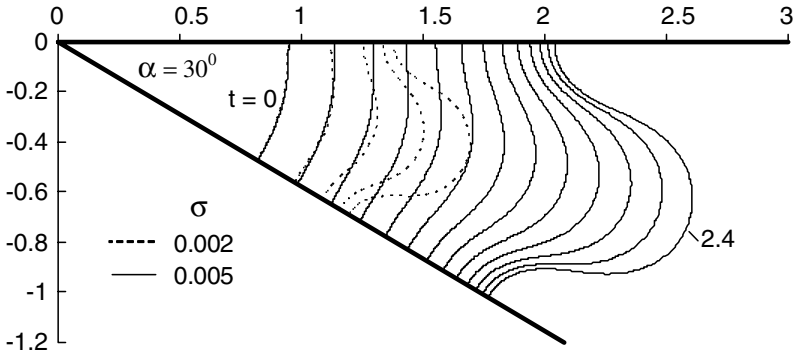

FIGURE 8. Effect of surface tension on the evolving free boundary in the corner $\alpha = -\pi/6$, with the sink $q = \alpha$ at infinity $\sigma = 0.002$ ($\cdots$) and $\sigma = 0.005$ (—). The initial shape corresponds to $C = 0.1\alpha$ and $k = 1$ in equations (3.2), (3.3).

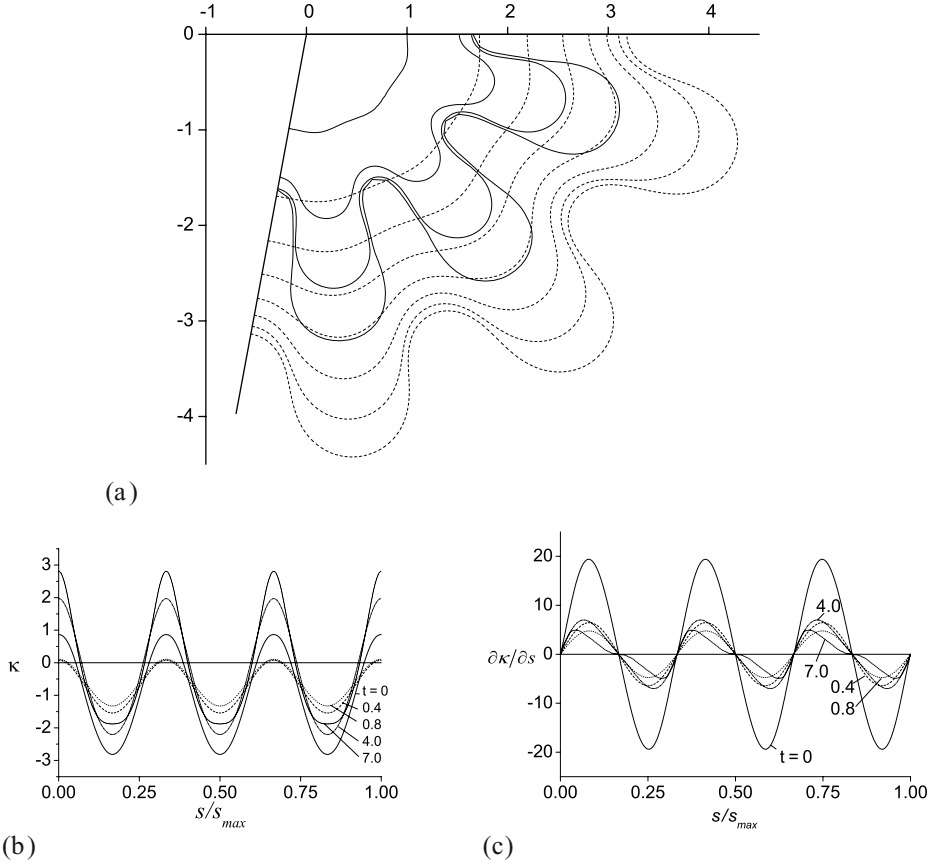

FIGURE 9. Flow in the corner $\alpha = -5\pi/9$: (a) evolution of the free boundary for $\sigma = 0.005$ (solid curves) and $\sigma = 0.01$ (broken curves), with time interval 1.0 between successive contours; and the corresponding curvature (b) and its derivative (c) for $\sigma = 0.01$. The initial free boundary is given by equations (3.2), (3.3) with $C = 0.1\alpha$ and $k = 3$.

https://doi.org/10.1017/S0956792506006759 Published online by Cambridge University Press

of the form $r = R_0(t) + \epsilon B(t)\cos n\theta + O(\epsilon^2)$, satisfy

$$\frac{dB}{dt} = \frac{(n-1)}{R_0^2}\left(\frac{q}{\alpha} - \frac{n(n+1)\sigma}{R_0}\right)B \tag{3.4}$$

(c.f. Paterson [35] equation (11)). Thus the growing interface is unstable if $R_0 > n(n+1)\sigma\alpha/q \equiv n(n+1)\sigma$, if, as we do for convenience, one takes $|q| = |\alpha|$. For our calculations the appropriate wavenumber is $n = 2\pi k/|\alpha|$ (since we are in a wedge rather than unconfined radial geometry this is not necessarily an integer), and for most of our examples the instability criterion is satisfied at the outset, thus fingers develop from the start, those with higher values of σ exhibiting slower growth as anticipated by (3.4). For the calculation of Figure 9 however, $|\alpha| = 5\pi/9$, $k = 3$ and $\sigma = 0.005$ gives $R_0 > 0.637$ as the criterion for instability, while $|\alpha| = 5\pi/9$, $k = 3$ and $\sigma = 0.01$ gives $R_0 > 1.27$ as the criterion, and in this case we do observe that, while the lower value of surface tension is unstable from the start, the higher value is clearly stabilised initially.

Figure 9(a) shows evolution in the same corner $\alpha = -5\pi/9$, for two larger values of the surface tension. The initial shape is given by (3.2), (3.3) with amplitude $C = 0.1\alpha$ and wave number $k = 3$. It can be seen that fingers develop for $\sigma = 0.005$, while for $\sigma = 0.01$ the free boundary smooths, as explained by the earlier remarks about linear stability. This smoothing is also apparent from the plot of curvature versus arc length in Figure 9(b). The initial maximum/minimum of the curvature decreases rapidly in magnitude at first, and then changes more weakly with time as the stability threshold is reached. We note again the fixed nodes in $\partial\kappa/\partial s$ in Figure 9(c), showing that the central (starlike) symmetry of the free surface is preserved in time. Consideration of the plots of κ and $\partial\kappa/\partial s$ for $\sigma = 0.01$ here reveals that we are far from the tip-splitting phenomenon in this example.

The evolution for $\sigma = 0.01$ and the "asymmetric" initial shape (relative to the nodes where $\partial\kappa/\partial s = 0$) given by (3.2) with slope

$$\delta(s) = \alpha\left(1 - s/s_{\max}\right) + C\sin\left(2\pi(3s)/s_{\max}\right) + C\sin\left(2\pi(2s)/s_{\max}\right), \tag{3.5}$$

is shown in Figure 10. The harmonic with wave number 3 is rapidly suppressed (this harmonic is stable for $R_0 < 1.27$), and only two fingers develop (the unstable $n = 2$ mode). The points $s/s_{max} = 0, 0.5, 1$ where $\partial\kappa/\partial s = 0$ (corresponding to the three initial fjords) maintain their positions for all time, while those points corresponding to the tips rapidly change position for $0 < t < 1$. As tip-splitting is approached, these curvature extrema approach the locations $(s/s_{max} \approx 0.25, 0.75)$, and once they have changed type from fingertips to fjords, they remain essentially fixed at these positions. An asymmetry of the fingers can be seen in Figure 10(a), and also in the corresponding curvature (and derivative) in Figures 10(b) and (c).

Finally, results for the case of a sink at the corner vertex are shown in Figure 11. The initial shape is given by equation (3.2), (3.3) with $C = -0.1\alpha$ (the the dash-dotted line in the figure is a circular arc, included for comparison). Although the chosen values of surface tension, $\sigma = 0.005$ and $\sigma = 0.05$, differ by a factor of 10, and the interface is

https://doi.org/10.1017/S0956792506006759 Published online by Cambridge University Press

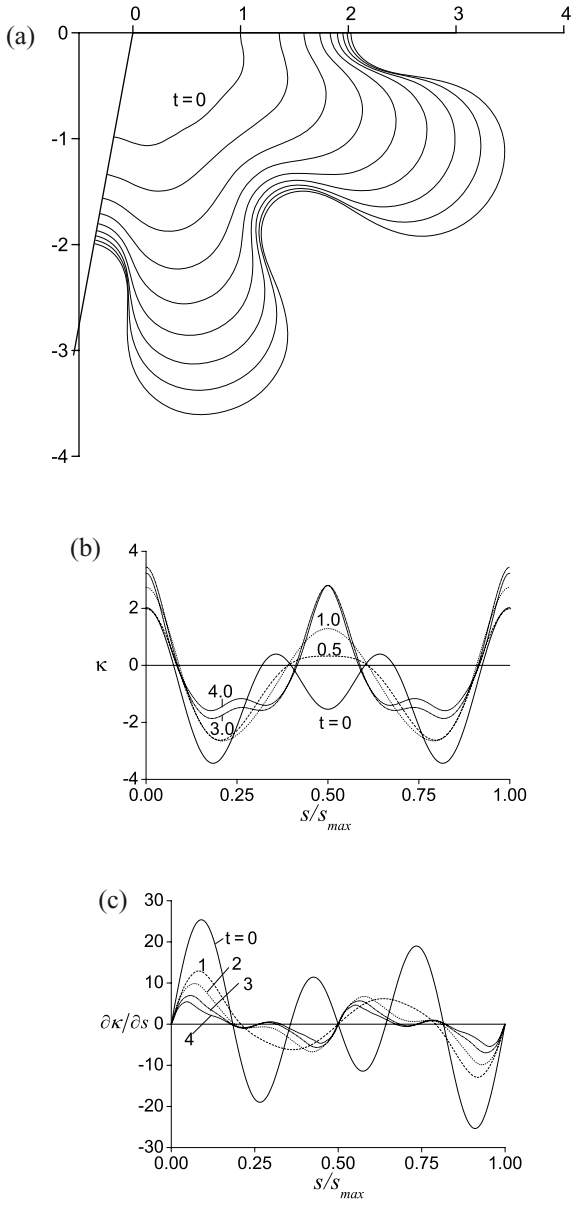

FIGURE 10. Flow in the corner $\alpha = -5\pi/9$ with $\sigma = 0.01$: (a) free boundary evolution, with time interval 0.5 between successive contours; and the corresponding evolution of the curvature (b) and its derivative (c). The initial shape of the free boundary is given by equation (3.5) with $C = 0.1\alpha$.

clearly unstable right from the start[2], until time $t \approx 1.6$ the calculated interface shapes are almost the same. Once the central finger has started to form, with the interface

[2] In this case linear stability analysis leads to an interface growth rate

$$\frac{\dot{B}}{B} = \frac{n+1}{R_0^2}\left(\frac{(-q)}{\alpha} - \frac{\sigma n(n-1)}{R_0}\right)$$

replacing (3.4).

https://doi.org/10.1017/S0956792506006759 Published online by Cambridge University Press

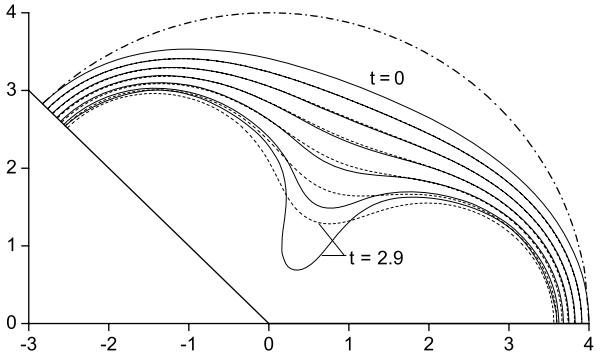

FIGURE 11. Evolution of the free boundary in the corner $\alpha = 3\pi/4$ with the sink at the vertex with $\sigma = 0.005$ (solid) and $\sigma = 0.05$ (dashed). The initial free boundary is given by equations (3.2) and (3.3) with $C = -0.1\alpha$, and the time interval between successive contours is 0.5.

becoming non-convex, the finger with the lower surface tension value grows fastest, as expected.

For completeness we note that similar results based on sophisticated numerical methods were obtained by Ceniceros *et al.* [7], Kelly & Hinch [25] and Nie & Tian [33], who studied the related problem of an initially-circular fluid domain with off-centre suction. In these papers also a finger forms in the evolving interface as suction proceeds, and for very small values of the surface tension parameter it is found that the finger tip (the free boundary) approaches the sink in the form of a wedge (the angle of which appears to be uniquely selected as the surface tension parameter goes to zero). Similarity solutions to the zero surface tension sink problem in the corner geometry (the appropriate local problem to study for this wedge-like free boundary behaviour) were found by Ben Amar [4, 5] who, with Combescot [8], later investigated the wedge angle selection issue. This was also later considered by Cummings & King [11], who provided some analysis of the solution breakdown mechanics in this problem. Although for small surface tension the free boundary is wedge-like as the sink is approached, it turns out that ultimately nonzero surface tension, however small, is always important (indeed, dominant), and in fact solution breakdown must occur via the free boundary moving in towards the sink in a locally flat (straight line) configuration.

3.1 Different contact angles $\gamma \neq \pi/2$

Finally, we briefly mention the case of different (acute) contact angles $\gamma \neq \pi/2$ within the fluid. This is not a major focus of our study, so we provide just one example, for completeness and to demonstrate that our methods can be extended to this case also. A simulation in a wedge of angle $\alpha = -5\pi/9$ (an air bubble at the wedge apex with suction of fluid from infinity) is given in Figure 12, for the initial free boundary given by (3.2) with slope $\delta(s)$ given by

$$\delta(s) = \alpha + \gamma + (\pi - \alpha - 2\gamma)s/s_{\max} + C\sin(2\pi k s/s_{\max}),$$

with $C = 0.1\alpha$ and $k = 2$. In this case the velocity at the contact points turns out to be very small from the outset, thus for convenience in this simulation the reference velocity

https://doi.org/10.1017/S0956792506006759 Published online by Cambridge University Press

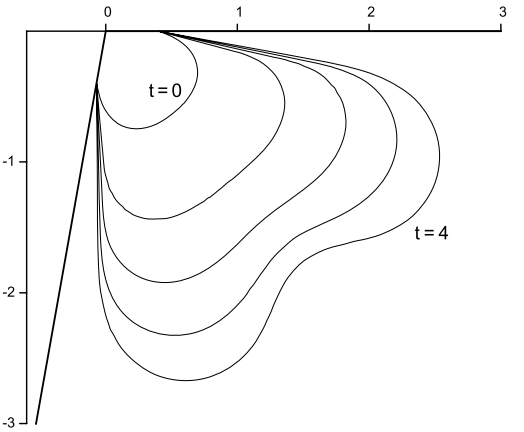

FIGURE 12. Evolution of the free boundary in a wedge of angle $\alpha = -5\pi/9$ with contact angle $\gamma = \pi/10$ and surface tension parameter $\sigma = 0.005$.

$v_O(t)$ that appears in formulae (2.9), (2.25) was changed to be the velocity of the free boundary on the centreline of the wedge. This scenario may be compared to the ZST free boundary problem studied by King *et al.* [26]. These authors consider flow driven by suction (or blowing) from infinity in a fluid domain initially in the shape of an infinite wedge of internal angle ϕ at the apex A. If one identifies the centreline of their fluid wedge with a rigid impermeable wall then their problem is a ZST local analogue of ours near the contact line between fluid and wall, with wedge half-angle $\phi/2$ corresponding to our contact angle γ. The case we present in Figure 12 corresponds to an angle $\phi \in (0, \pi/2)$ in their analysis, in the suction case, for which they conjecture[3] the following result: "(S1) For $0 < \phi \leqslant \pi/2$ it is possible for the solution to exist. The boundary Γ continues to have a corner of angle ϕ at A." (That is, the free boundary does not move away from the point A under the suction.) Our numerical observations at small surface tension ($\sigma = 0.005$) for the NZST problem are thus entirely consistent with this ZST conjecture.

4 Conclusion

We have presented a new method for solving the free-boundary problem of unsteady Hele–Shaw flows with surface tension, driven by injection or suction mechanism in a corner geometry. Our method allows for either a source or a sink, located at the origin or at infinity. Our approach is based on the determination of two governing functions: the complex velocity, and the derivative of the complex potential defined in an auxiliary parameter domain. The analytical expression for the (time-dependent) function mapping the parameter domain onto the physical domain is found using these governing functions.

Using the obtained mapping function we derived an integral equation for the function of the velocity modulus on the free boundary, which shows that the velocity modulus is determined by the curvature of the free boundary (and its first and second derivatives) at each moment of time.

[3] Their conjectures for the suction case are based on time-reversal arguments from the blowing problem, for which they present formal asymptotic results.

https://doi.org/10.1017/S0956792506006759 Published online by Cambridge University Press

The numerical results presented show the interface dynamics for various initial shapes of the free boundary in both converging and diverging channels for unstable sink-driven flow. For a sink at infinity, the results confirm the linear stability analysis of Paterson [35] and in the nonlinear regime, reproduce the development of radial fingering and tip-splitting, as seen in earlier experiments [29, 35, 42].

Our approach may be compared with that taken by Dai & Shelley [12] and Hou *et al.* [20]. These authors used the Plemelj formulae for the complex velocity, and obtained a Birkhoff-Rott integral in which the vortex sheet strength is determined from a Fredholm integral of the second kind. At each timestep (using an implicit timestepping scheme) they need to solve the Fredholm integral equation, and evaluate the Birkhoff–Rott integral using a Hilbert transform. In our method, on the other hand, the obtained integral equation (2.25) was solved just by direct application of the Hilbert transform. The price of this simplicity and ease of implementation is the need for a smaller timestep of integration, as we can use only an explicit time integration method. To apply an implicit method we would need to derive an integral equation with respect to the time derivative of the velocity modulus on the free boundary, from the kinematic equation in the parametric plane, (2.31). We note, however, that the stability constraint on the timestep for our explicit scheme is not a limitation for long-time predictions. For a smaller timestep, a smaller number of iterations are required to solve the nonlinear integral equation, so in fact the total calculation time depends only weakly on the timestep.

Acknowledgements

Both authors gratefully acknowledge the London Mathematical Society and the University of Nottingham for supporting YAS's visit to the UK. LJC thanks the National Grid plc for generous financial support in the form of a sponsored Royal Society Dorothy Hodgkin Fellowship. YAS thanks John Ockendon for helpful discussions during a visit to Oxford University.

Appendix A Demonstration that $\partial v/\partial \eta = 0$ at wall intersection points

Consider the flow local to the contact point O, sketched in figure A 1. Let $v_b = ve^{i\beta}$ be the local (complex) free boundary velocity, then

$$v_b = \dot{z}_b$$

for points $z_b(s,t)$ on the boundary. The complex tangent vector along $\Gamma(t)$ satisfies

$$\frac{\partial z_b}{\partial s} = e^{i(\pi-\gamma)} = -e^{-i\gamma}.$$

Thus,

$$\frac{\partial}{\partial s}(\dot{z}_b) = -\frac{d}{dt}(e^{-i\gamma}) = i\dot{\gamma}e^{-i\gamma} = \frac{\partial v_b}{\partial s},$$

and it follows that, if $\dot{\gamma} = 0$ as we assume, then $\partial v_b/\partial s = 0$, and hence $\partial v/\partial s = 0$ at O (and A). Since $\partial/\partial\eta = (ds/d\eta)\partial/\partial s$, and $|ds/d\eta| < \infty$ in the conformal mapping near O,

https://doi.org/10.1017/S0956792506006759 Published online by Cambridge University Press

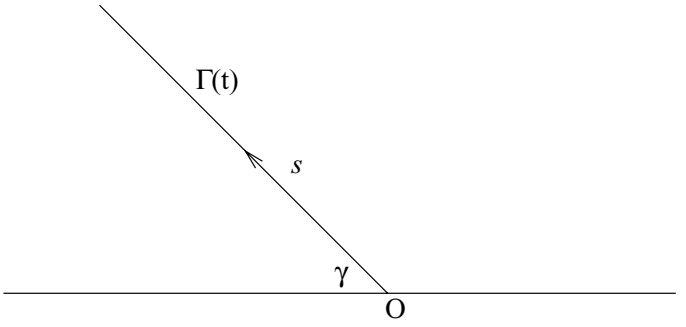

FIGURE A 1. Local behaviour near the contact point O.

we deduce that

$$\frac{\partial v}{\partial \eta} = 0 \quad \text{at the point } O, \tag{A 1}$$

as claimed.

References

[1] BATAILLE, J. (1968) Stability of a radial immiscible drive. *Revue Inst. Petrole*, **23**, 1349–1364
[2] BEAR, J. (1972) *Dynamics of fluids in porous media.* New York. Elsevier.
[3] BEN AMAR, M., PELCÉ, P. & TABELING, P. (editors) (1991) *Growth and Form: nonlinear aspects. NATO Advanced Study Institute on nonlinear phenomena related to Growth and Form.* New York. Plenum Press.
[4] BEN AMAR, M. (1991) Exact self-similar shapes in viscous fingering. *Phys. Rev. A*, **43**, 5724–5727.
[5] BEN AMAR, M. (1991) Viscous fingering in a wedge. *Phys. Rev. A*, **44**, 3673–3685.
[6] BRENER, E. A., KESSLER, D. A., LEVINE, H. & RAPPEL, W.-J. (1990) Selection of the viscous finger in the 90^{O} geometry. *Europhys. Lett.* **13**, 161–166.
[7] CENICEROS, H. D., HOU, T. Y. & SI, H. (1999) Numerical study of Hele-Shaw flow with suction. *Phys. Fluids*, **11**, 2471–2486.
[8] COMBESCOT, R. & BEN AMAR, M. (1991) Selection of Saffman-Taylor fingers in the sector geometry. *Phys. Rev. Lett.* **67**, 453–456.
[9] COMBESCOT, R., HAKIM, V., DOMBRE, T., POMEAU, Y. & PUMIR, A. (1986) Shape selection for Saffman-Taylor fingers. *Phys. Rev. Lett.* **56**, 2036–2039.
[10] COMBESCOT, R. (1992) Saffman-Taylor fingers in the sector geometry. *Phys. Rev. A*, **45**, 873–884.
[11] CUMMINGS, L. J. & KING, J. R. (2004) Hele-Shaw flow with a point sink: generic solution blow-up. *Euro. J. Appl. Math.* **15**, 1–37.
[12] DAI, W.S. & SHELLEY, M. J. (1993) A numerical study of the effect of surface tension and noise on an expanding Hele-Shaw bubble. *Phys. Fluids A*, **5**, 2131–2146.
[13] DIBENEDETTO, E., FRIEDMAN, A. 1984 The ill-posed Hele-Shaw model and the Stefan problem for supercooled water. *Trans. Amer. Math. Soc.* **282**, 183–204.
[14] GALIN, L. A. (1945) Unsteady filtration with a free surface. *Dokl. Akad. Nauk. S.S.S.R.* **47**, 246–249.
[15] GILLOW, K. & HOWISON, S. D. (n.d.) Bibliography of free and moving boundary problems in Hele-Shaw and Stokes flow. At http://www.maths.ox.ac.uk/~howison/Hele-Shaw/
[16] GUREVICH M. I. (1965) *Theory of Jets in Ideal Fluids.* New York. Academic. Press. 380.

https://doi.org/10.1017/S0956792506006759 Published online by Cambridge University Press

[17] Hele-Shaw, H. S. (1898) The flow of water. *Nature*, No. 1489, **58**, 34–36.
[18] Helmholtz, H. (1868) Ueber discontinuirliche Flussigkeitsbewegungen. Monatsber. Konigl. Akad. Wissenschaften, Berlin.
[19] Hong, D. C. & Langer, J. S. (1986) Analytic theory for the selection of Saffman-Taylor fingers. *Phys. Rev. Lett*. **56**, 2032–2035.
[20] Hou, T. Y., Lowengrub, J. S. & Shelley, M. J. (1994) Removing the stiffness from interfacial flows with surface tension. *J. Computational Physics*, **114**, 312–338.
[21] Howison, S. D. (1986) Fingering in Hele-Shaw cells *J. Fluid Mech.* **167**, 439–453.
[22] Howison, S. D. (1992) Complex variable methods in Hele-Shaw moving boundary problems. *Europ. J. Appl. Math.* **3**, 209–224.
[23] Howison, S. D. & King, J. (1989) Explicit solutions to six free-boundary problems in fluid flow and diffusion. *IMA J. Appl. Math.* **42**, 155–175.
[24] Howison, S. D., Ockendon, J. R. & Lacey, A. A. (1985) Singularity development in moving boundary problems. *Q. J. Mech. Appl. Math.* **38**, 343–360.
[25] Kelly, E. D. & Hinch, E. J. (1997) Numerical simulations of sink flow in the Hele-Shaw cell with small surface tension. *Europ. J. Appl. Math.* **8**, 533–550.
[26] King, J. R., Lacey, A. A. & Vazquez, J. L. (1995) Persistence of corners in free boundaries in Hele-Shaw flow. *Europ. J. Appl. Math.* **6**, 455–490.
[27] Kirchhoff, G. (1869) Zur Theorie freier Flussigkeitsstrahlen. *Borchardt's Journ., Bd. 70.*
[28] Lacey, A. A. (1982) Moving boundary problems in the flow of liquid through porous media. *J. Austral. Math. Soc. (Series B)*, **24**, 171–193.
[29] Lajeunesse, E. & Couder, Y. (2000) On the tip-splitting instability of viscous fingers. *J. Fluid Mech.* **419**, 125–149.
[30] McGeough, J. A. (1974) *Principles of electrochemical machining*. Chapman & Hall.
[31] McLean, J. W. & Saffman, P. G. (1981) The effect of surface tension on the shape of fingers in a Hele-Shaw cell. *J. Fluid Mech.* **102**, 455–469.
[32] Miranda, J. A. & Widom, M. (1998) Radial fingering in a Hele-Shaw cell: a weakly nonlinear analysis. *Physica D* **120**, 315–328.
[33] Nie, Q. & Tian, F. R. (1998) Singularities in Hele-Shaw flows. *SIAM J. Appl. Math.* **58**, 34–54.
[34] Ockendon, J. R., Howison, S. D., Lacey, A. A. & Movchan, A. B. (2003) *Applied Partial Differential Equations (revised edition)*. Oxford University Press.
[35] Paterson, L. (1981) Radial fingering in a Hele-Shaw cell. *J. Fluid Mech.* **113**, 513–529.
[36] Polubarinova-Kochina, P. Ya. (1945) On the motion of the oil contour. (In Russian.) *Dokl. Akad. Nauk. S.S.S.R.* **47**, 254–257.
[37] Polubarinova-Kochina, P. Ya. (1962) *Theory of groundwater movement*. Princeton University Press.
[38] Rubinstein, L. I. (1971) *The Stefan problem.* American Mathematical Society, Providence.
[39] Saffman, P. G. & Taylor, G. I. (1958) The penetration of a fluid into a porous medium or Hele-Shaw cell containing a more viscous liquid. *Proc. Roy, Soc. Lond. A*. **245**, 312–329.
[40] Semenov, Yu. A. & Cummings L. J. (2005) General solution for two-dimensional corner flows under Darcy's law. *Int. J. Fluid Mech. Res.* **32**, 420–438.
[41] Shraiman, B. I. (1986) Velocity selection and the Saffman-Taylor problem. *Phys. Rev. Lett*. **56**, 2028–2031.
[42] Thomé, H., Rabaud, M., Hakim, V. & Couder, Y. (1989) The Saffman-Taylor instability: From the linear to the circular geometry. *Phys. Fluids A*, **1**, 224–240.
[43] Zhukovskii, N. E. (1890) Modification of Kirchhoff's method for determination of a fluid motion in two directions at a fixed velocity given on the unknown streamline. (In Russian.) *Matemat. sbornik* **XV**.